HHS Public Access

Author manuscript

Nat Nanotechnol. Author manuscript; available in PMC 2012 April 01.

Published in final edited form as:

Nat Nanotechnol. ; 6(10): 658–667. doi:10.1038/nnano.2011.105.

Thermodynamically Stable RNA three-way junctions as platform for constructing multi-functional nanoparticles for delivery of therapeutics

Dan Shu[1,†], **Yi Shu**[1,†], **Farzin Haque**[1,†], **Sherine Abdelmawla**[2,3], and **Peixuan Guo**[1,*]

[1] Nanobiomedical Center, University of Cincinnati, Cincinnati, OH 45267

[2] Kylin Therapeutics, Inc, West Lafayette, IN 47906

[3] Bindley Bioscience Center, Purdue University, West Lafayette, IN 47906

Abstract

RNA nanoparticles can potentially be used to treat cancers and viral infection but their instability has hindered their therapeutic applications. The lack of covalent linkage or cross-linking in the nanoparticles causes dissociation in vivo. Here we show the assembly of thermodynamically stable three-way junction (3WJ) of the motor pRNA of bacteriophage phi29 from 3–6 pieces of RNA oligomers without the use of metal salts to form stable multifunctional nanoparticles. Each RNA oligomer contains either a receptor-binding ligand, aptamer, siRNA or ribozyme functional module. When mixed together, they self-assemble into tri-stars nanoparticles with a 3WJ core. The nanoparticles are resistant to 8M urea denaturation, stable in serum and remain intact at extremely low concentrations. The modules remain functional in vitro and in vivo, suggesting the 3WJ core can be used as a platform for building a variety of multifunctional nanoparticles. Of the 25 different 3WJ motifs evaluated, only one other motif in biological RNA shares similar characteristics as the phi29 3WJ.

Living organisms produce an assortment of highly ordered structures composed of DNA, RNA and proteins to perform diverse functions. DNA has been used as biomaterials[1] but RNA, which share common properties with DNA, has received less attention[2–4]. RNA is attractive because it possesses non-canonical base-pairing and catalytic function similar to some proteins[2] and yet like DNA, it can be easily manipulated. Typically, RNA molecules contain a large variety of single-stranded stem-loops for inter- and/or intra-molecular interactions[5]. These loops serve as mounting dovetails, which eliminates the need for

*Address correspondence to: Peixuan Guo, Rm 1436, ML #0508, Vontz Center for Molecular Studies, 3125 Eden Avenue, University of Cincinnati, Cincinnati, OH 45267, USA, guopn@ucmail.uc.edu, Phone: (513)558-0041, Fax: (513)558-6079.

†Co-first authors contributed equally to this work.

ADDITIONAL INFORMATION

Supplementary information accompanies this paper at: www.nature.com/naturenanotechnology.

Reprints and permission information is available online at: http://npg.nature.com/reprintsandpermissions/.

AUTHOR CONTRIBUTIONS

P.G. conceived, designed and led the project; D.S., Y.S., and F.H. designed and conducted the *in vitro* experiments; S.A. performed animal imaging experiments; P.G., D.S., Y.S., and F.H. analyzed the data and co-wrote the manuscript.

external linking dowels during fabrication and assembly[3,6]. Since the discovery of siRNA[7], nanoparticles of siRNA[8–10], ribozymes[11–13], riboswitch[14,15], miRNA[16–18] have been explored for the treatment of cancers and viral infections.

One of the challenges in the field of RNA nanotechnology is the relative instability of the nanoparticles; lack of covalent binding or cross-linking in the particles causes dissociation at ultra low concentrations in the animal and human circulation systems after systemic injection. This has hindered the efficiency of delivery and therapeutic applications of RNA nanoparticles[2]. Although it is not absolutely necessary for RNA helix formation, tens of mM of magnesium is required for optimum folding of nanoparticles such as phi29 pRNA[19,20]. Because the concentration of magnesium under physiological conditions is generally less than 1mM, misfolding and dissociation of nanostructures that use RNA as a scaffold can occur at such low concentrations.

The DNA packaging motor of bacteriophage phi29 is geared by a pRNA ring[21], which contains two functional domains[22,23]. The central domain of a pRNA subunit contains two interlocking loops, denoted as right- and left-handed loops, that can be engineered to form dimers, trimers or hexamers[3,24,25]. Because the two domains fold separately, replacing the helical domain with a siRNA does not affect the structure, folding or intermolecular interactions of the pRNA[23,26,27]. Such a pRNA/siRNA chimera has been shown to be useful for gene therapy[8–11]. The two domains are connected by a three-way junction (3WJ) region (Fig 1d) and this unique structure has motivated its use in RNA nanotechnology. Here we show that the 3WJ region of the pRNA can be assembled from three pieces of small RNA oligomers with high affinity. The resulting complex is stable and resistant to denaturation in the presence of 8M urea. Incubation of three RNA oligomers, with each carrying either a siRNA, a receptor binding aptamer or a ribozyme, resulted in trivalent RNA nanoparticles that are suited as therapeutic agents. Of the 25 3WJ motifs obtained from different biological systems, we found the pRNA 3WJ most stable.

Properties of the 3WJ-pRNA

The 3WJ domain of phi29 pRNA was constructed using three pieces of RNA oligos denoted a_{3WJ}, b_{3WJ}, and c_{3WJ} (Fig. 1d). Two of the oligos a_{3WJ}, and c_{3WJ} were resistant to staining by ethidium bromide (Fig. 2a) and weakly stained by SYBR Green-II, while c_{3WJ} remained unstainable (Fig. 2a). Ethidium bromide is an intercalating agent that stain dsRNA and dsDNA or ssRNA containing secondary structures or base-stacking. SYBR Green II stains both ss- and ds-RNA or DNA. The absence or weak staining indicates novel structural properties.

The mixing of three oligos a_{3WJ}, b_{3WJ}, and c_{3WJ} at 1:1:1 stoichiometric ratio at room temperature in distilled water resulted in high efficient formation of the 3WJ domain. Melting experiments suggest that the three components of the 3WJ-pRNA core (T_m of 58°C) have a much higher affinity to interact favorably in comparison with any of the two components (Fig. 2b). The 3WJ domain remained stable in distilled water without dissociating at room temperature for weeks. If one of the oligos was omitted (Fig. 2a, lanes 4–6), dimers were observed, as exhibited by faster migration rates compared to the 3WJ

domain (Fig. 2a, lane 7). Generally, dsDNA and dsRNA are denatured and dissociate in presence of 5M[28] or 7M urea[29]. In the presence of 8M urea, the 3WJ domain remained stable without dissociation (Fig. 2d), thereby demonstrating its robust nature.

The length of the helices H1, H2 and H3 were 8, 9, and 8 base-pairs, respectively. RNA complexes with the deletion of 2 base-pairs in H1 and H3 (Fig. 1d, Fig. 2d) seems to have no effect on complex formation (Fig. 2d, lanes 8, 9). However, deletion of 2 base-pairs at H2 (Fig. 1d, Fig. 2d), did not affect the formation of the complex, but made the 3WJ domain unstable in the presence of 8M urea (Fig. 2d, lanes 7, 10). These results demonstrate that while 6 base pairs are sufficient in two of the stem regions, 8 bases are necessary for H2 to keep the junction domain stable under strongly denaturing conditions.

To further evaluate the chemical and thermodynamic properties of 3WJ-pRNA, the same sequences were used to construct a DNA 3WJ domain. In native gel, when the three DNA oligos are mixed in a 1:1:1 ratio, the 3WJ-DNA assembled (Fig. 2e). However, the DNA 3WJ complex dissociated in the presence of 8M urea (Fig. 2e, bottom). DNA/RNA hybrid 3WJ domains exhibited increasing stability as more RNA strands were incorporated. In essence, by controlling the ratio of DNA to RNA in the 3WJ domain region, the stability can be tuned accordingly.

To assess the stability of the 3WJ-pRNA, we conducted competition experiments in the presence of urea and at different temperatures as a function of time. For a candidate therapeutic RNA nanoparticle, it is necessary to evaluate whether it would dissociate at physiological temperature of 37°C. A fixed concentration of the Cy3 labeled 3WJ-pRNA core was incubated with unlabeled b_{3WJ} at 25°C, 37°C, and 55°C, respectively. At 25°C, there is no exchange of labeled and unlabeled b_{3wj} (Fig. 3a); at physiological temperature of 37°C, only a very small amount of exchange is observed in the presence of 1000-fold higher concentration of labeled b_{3wj} (Fig. 3a); and at 55°C (close to the T_m of the 3WJ-pRNA), there is approximately half-and-half exchange at 10-fold excess and near-complete exchange at 1000-fold higher concentration of labeled b_{3wj} (Fig. 3a). The results are consistent with the T_m measurements.

A fixed concentration of the Cy3 labeled 3WJ-pRNA core was incubated with unlabeled b_{3WJ} at room temperature in presence of 0–6M urea. At equimolar concentrations (Cy3-[a b*c]$_{3WJ}$:unlabeled b_{3wj}=1:1), there was little or no exchange under all urea conditions investigated (Fig 3b). At five-fold higher concentration (Cy3-[ab*c]$_{3WJ}$:unlabeled b_{3wj}=1:5), there was little or no exchange under 2M and 4M urea conditions; and ~20% exchange at 6M-urea (Fig 3b). So, 6M urea ‘destabilizes’ the 3WJ-pRNA complex only to an insignificant extent.

Construction and properties of 3WJ-pRNA with therapeutic modules

It has been previously demonstrated that the extension of the phi29 pRNA at the 3′-end does not affect the folding of pRNA global structure[26]. The sequences of the three RNA oligos a_{3WJ}, b_{3WJ}, and c_{3WJ}, were placed at the 3′-end of the pRNA monomer, Ab′. Mixing of the three resulting pRNA chimeras containing a_{3WJ}, b_{3WJ}, and c_{3WJ} sequences respectively, at equimolar concentrations led to the assembly of 3WJ branched nanoparticles harboring one

pRNA at each branch. AFM images strongly confirmed the formation of larger RNA complexes with three-branches (Fig. 1e, f), which were consistent with gel shift assays (Fig. 3c). This nanoparticle can also be co-transcribed and assembled in one step during transcription with high yield (data not shown).

When RNA nanoparticles are delivered systemically to the body, the particles will exist in low concentrations due to dilution by circulating blood. Only those RNA particles that are intact at low concentrations can be considered as therapeutic agents for systemic delivery. To determine whether the larger structure with three branches harboring multi-module functionalities are subjected to dissociation at low concentration, this [^{32}P]-labeled complex was serially diluted to extremely low concentrations. It was found that the concentration for dissociation was below the detection limit of the [^{32}P]-labeling technology. Even at 160 pM in TMS buffer, the lowest concentration tested, the dissociation of the nanoparticles was undetectable (Fig. 3c).

Multi-module RNA nanoparticles were constructed using this 3WJ-pRNA domain as a scaffold (Fig. 4a). Each branch of the 3WJ carried one RNA module with defined functionality, such as a cell receptor binding ligand, aptamer, siRNA, ribozyme. The presence of the modules or therapeutic moieties did not interfere with the formation of the 3WJ domain, as demonstrated by AFM imaging (Fig. 4c). Furthermore, the chemically modified (2′-F U/C) 3WJ-pRNA complex harboring three monomeric pRNAs were resistant to degradation in cell culture medium with 10% serum even after 36 hours of incubation, while the unmodified RNA degraded within 10-min (Supplementary Fig.3).

In vitro and *in vivo* assessments of 3wj-pRNA with therapeutic modules

Making fusion complexes of DNA or RNA is not difficult, but ensuring the appropriate folding of individual modules within the complex after fusion is not a simple task. To test whether the incorporated RNA moieties retain their original folding and functionality after being fused and incorporated, Hepatitis B virus (HBV) cleaving ribozyme[11] and MG (Malachite Green dye, triphenylmethane) binding aptamer[30] were used as model systems for structure and function verification. The free MG is not fluorescent by itself, but emits fluorescent light after binding to the aptamer.

It was found that the HBV ribozyme was able to cleave its RNA substrate after being incorporated into the nanoparticles (Fig. 4d) and the fused MG-binding aptamer retained its capacity to bind MG, as revealed by its fluorescence emission (Fig. 4f). The activity results are comparable to optimized positive controls and therefore confirm that individual RNA modules fused into the nanoparticles retained their original folding after incorporation into the RNA nanoparticles.

Many kinds of cancer cell lines, especially from the epithelial origin, overexpress the folate receptor on the surface elevated by thousand fold. Folate has been used extensively as a cancer cell delivery agent via folate receptor-mediated endocytosis[31]. The 2′-F U/C modified fluorescent 3WJ-pRNA nanoparticles with folate conjugated into one of its branches complex were tested for its cell binding efficiency. One fragment of 3WJ-pRNA core was labeled with the folic acid for targeted delivery[10], the second fragment was labeled

with Cy3, and the third fragment was fused to the siRNA that can silence the gene of the anti-apoptotic factor, surviving[32]. Negative controls included the RNA nanoparticles contained folate but scramble siRNA sequence; and 3WJ-pRNA core with active siRNA but without folate. Flow cytometry data revealed that the folate-3WJ-pRNA nanoparticles bound and loaded its siRNA to the cell with almost 100% binding efficiency (Fig.5a, Supplementary Fig.4). Confocal imaging indicated a strong binding of the RNA nanoparticles and efficient entry into the targeted cells, as demonstrated by the excellent co-localization and overlap of the fluorescent 3WJ-pRNA nanoparticles (red) and cytoplasma (green) (Fig.5b).

Two 3WJ-RNA nanopartles were constructed for assaying gene silencing effect. Particle [3WJ-pRNA-siSur-rZ-FA] harbors folate and survivin siRNA, while [3WJ-pRNA-siScram-Rz-FA] harbors folate and Survivin siRNA scramble as control. After 48hrs transfection, both qRT-PCR and Western Blot assays confirmed reduced survivin gene expression level of 3WJ-pRNA-siSur-rZ-FA compared to the scramble control on both mRNA and protein levels. The silencing potency is comparable to the positive Survivin siRNA only control, albeit the reduction of both the RNA complexes was modest (Fig.5c).

Two of the key factors that may affect the pharmacokinetic (PK) profile are metabolic stability and renal filtration. It has been reported that regular siRNA molecules have extremely poor pharmacokinetic properties, since they have a short half-life ($T_{1/2}$) and fast kidney clearance due to both metabolic instability and small size (<10-nm)[33]. The PK profile of AlexaFluor647-2′-F-pRNA nanoparticles that use the 3WJ domain as a scaffold were studied in mice upon systemic administration of a single intravenous injection via the tail vein, followed by blood collection. The concentration of the fluorescent nanoparticle in serum was determined. The half-life ($t_{1/2}$) of the pRNA nanoparticles was determined to be 6.5~12.6 hours, compared to the control 2′F-modified siRNA, which could not be detected beyond 5 min post-injection, which is close to the $t_{1/2}$ of 35 mins reported in the literature[34].

To confirm that the RNA nanoparticles were not dissociated into individual subunits *in vivo*, RNA nanoparticles were constructed with one subunit carrying the folate to serve as a ligand for binding to the cancer cells, and the other subunit carrying a fluorescent dye. The nanoparticles were systemically injected into mice through the tail vein. Whole body imaging revealed that fluorescence was located specifically at the xenograpic cancer experssing the folate-receptor and was not detected in other organs in the body (Fig.5e), indicating that the particles did not dissociate *in vivo* after systemic delivery.

Comparing pRNA 3WJ with other 3WJ motifs in biological RNA

There are many 3WJ motifs in biological RNA, some of which are stabilized by extensive tertiary interactions and non-canonical base pairings and base stacking[35–40]. To assess whether the properties of the 3WJ-pRNA core are unique, we thoroughly investigated the assembly and stability of 25 3WJ motifs (Table 1 and Supplementary Table 2) reported in the literature[35,39,41–43]. It was found that 14 of the 25 motifs were impractical to study using core sequences, for example, some of them were too short (less than 10-nt for one of their fragments) for chemical synthesis. Using synthesized RNA fragments with the exact

sequences as reported, with appropriate controls, the other 11 motifs were thoroughly investigated. Only six of the 11 structures assembled into a 3WJ complex, based on gel-shift assays (Table 1 and Fig.6). However, in presence of 8M urea, only the 3WJ-pRNA core and 3WJ-5S rRNA core were stable. The Alu SRP appears to have assembled; however, with appropriate controls (Supplementary Fig.1), it was found that the band was from the strong folding of one individual RNA fragment (a_{3WJ}) by itself, rather than the assembly of a 3WJ.

Moreover, 25 different RNA nanoparticles were constructed using each of the central 3WJ motifs as the scaffold to test their potential for constructing RNA nanoparticles harboring three functionalities with extended sequences (Sup Fig.2). Here, we used individual phi29 pRNA subunits as modules[3,23–26]. The sequences for each of the three oligos comprising individual 3WJ were placed at the 3′-end of the 117-nt pRNA, thereby serving as sticky ends. Upon co-transcription (of three pRNA strands harboring the sticky end sequences of the 3WJ, respectively) 10 of the 25 constructs were able to assemble into a 3WJ complex via the sticky ends representing the three fragments of the 3WJ, as demonstrated by gel shift assays (Supplementary Fig.2). However, only 2 of the constructs (3WJ-pRNA and 3WJ-5S rRNA) were resistant to 8M urea denaturation, which is consistent with the RNA oligo assembly data (Fig.6). These results suggest that only the 3WJ-5S rRNA is comparable to the 3WJ-pRNA, and therefore, the 3WJ-5S rRNA can also serve as a platform to organize RNA modules bearing different functionalities.

To test whether the functionalities incorporated in the nanoparticles with the 3WJ core display catalytic or binding function, the HBV ribozyme and MG aptamer were incorporated into RNA nanocomplexes. Both the HBV ribozyme (Fig.4d, e) and the MG aptamer were functional after being incorporated into the 3WJ-pRNA or 3WJ-5S rRNA, respectively(Fig. 4f, g), suggesting that the 3WJ-5S rRNA is comparable to 3WJ-pRNA for constructing complexes harboring different RNA functionalities for cell delivery.

One of the most important parameters for evaluating therapeutic RNA nanoparticles is their thermodynamic stability under physiological conditions *in vivo*. T_m studies on three oligos for each of the 11 3WJ motif were conducted under the physiological buffer with 5-mM Mg and 100-mM NaCl at pH 7.6 (Fig.6 and Table 1). Among the assembled 3WJ structures, pRNA displayed the highest T_m of 58°C. The T_m closest to the 3WJ-pRNA was the 3WJ-5S rRNA with 54.3°C.

The affinity and efficiency of assembly was further investigated by both gel retardation assay and melting experiments (data only shown for 3WJ-pRNA (Fig.2a, b), 3WJ-5S rRNA and 3WJ-Alu SRP cores (Sup Fig.1). The 3WJ-pRNA displayed a very smooth high-slope temperature dependant melting curve, and clean bands in the gel, clearly displaying the assembly of monomer, dimer and 3WJ with little or no residual RNA fragments (Fig.2a, b). The results suggest that the three components of the 3WJ-pRNA have a much higher affinity to interact favorably in comparison with any of the two components. Furthermore, the sharp melting transition indicates cooperative simultaneous folding of the three helical stems. In contrast, the 3WJ-5S rRNA and all other 3WJ motifs displayed temperature dependant curves with lower slopes. Titration of the three oligos of the 3WJ-5S rRNA system revealed that mixing of only two of the three RNA fragments resulted in the formation of a urea

sensitive band with a migration rate even slower than the entire 3WJ complex (Sup Fig.1). This suggests that the individual fragment or their two-fragment combination of the 3WJ-5S rRNA might have undesired binding affinities that interfere with the final 3WJ assembly. Nevertheless, the affinity of the three-component interaction is sufficiently higher than the two-component interaction in the 3WJ-5S rRNA system to drive the assembly of the final 3WJ structure. For Alu SRP, the folding of the individual strands significantly interferes with the formation of the 3WJ and hence the complex does not assemble (Supplementary Fig.1).

Although systematic comparison of assembly and stability of different 3WJs has not been studied, several studies concerning the T_m measurements of individual 3WJ motifs have been reported[44–48]. Some studies elucidate the thermodynamic factors that govern the folding of 3WJ RNA motifs, such as the hairpin ribozyme[45] and intact stem-loop mRNA[46]. Thermodynamic parameters of a variety of constructs (mutations and insertions) based on the structure and sequence of the 3Wj core of 5S-rRNA have been reported[44,47,48]. They utilized a two-strand system instead of the three fragments approach, and hence the results are not directly comparable. Nevertheless, their results are consistent with our findings.

In conclusion, these results suggest that the phi29 3WJ domain has the potential to serve as a platform for the construction of RNA nanoparticles containing multiple functionalities for the delivery of therapeutics to specific cells for the treatment of cancer, viral infection, and genetic diseases. We thoroughly evaluated 25 3WJ motifs in biological RNA and identified 3WJ-5S rRNA as the only 3WJ motif comparable to 3WJ-pRNA for constructing complexes harboring different functionalities.

EXPERIMENTAL PROCEDURES

Construction of multi-module RNA nanoparticles

Sequences for each of the RNA strands a_{3wj}, b_{3wj}, and c_{3wj} were added to the 3′-end of each 117-nt pRNA-Ab′ (Fig. 1e). The pRNA-a_{3WJ}, pRNA-b_{3WJ}, and pRNA-c_{3WJ} were then synthesized *in vitro* by transcription of the corresponding DNA template by the T7 RNA polymerase. The 3WJ-pRNA harboring three monomeric pRNA were then self-assembled by mixing the three subunits in equal molar concentrations. Alternatively, the three individual templates can be co-transcribed and assembled in one step followed by purification in 8% native PAGE gel.

The sequences for the siRNA, HBV ribozyme, malachite green (MG) binding aptamer and folate labeled RNA were rationally designed with the sequences of the strands a_{3WJ}, b_{3WJ}, and c_{3WJ}, respectively (Fig. 4, Supplementary Table 2). Multi-module 3WJ-pRNA-HBV ribozyme-Survivin siRNA-folate (3WJ-pRNA-siSur-Rz-FA) or 3WJ-pRNA-MG aptamer-Survivin siRNA-folate (3WJ-pRNA-siSur-MG-FA) was assembled from four individual fragments including a 26-nt folate-labeled RNA (Trilink) or folate-DNA strand (synthesized in house); and, chemically synthesized 21-nt siRNA or scramble siRNA anti-sense strand (IDT). The 106-nt strand harboring HBV ribozyme sequence or 96-nt strand harboring MG binding aptamer and the 41-nt strand holding the folate-DNA/RNA were transcribed from DNA template amplified by PCR (Supplementary Table 2). Fluorescent dyes were labeled

on the 106-nt RNA strand by using the Label IT® siRNA Tracker Intracellular Localization Kit, Cy3™ (Mirus Bio LLC). The four RNA strands were mixed after purification in TMS buffer at equal molar ratio and then heated up to 80°C for 5 mins, followed by slow cooling to 4°C. The assembled nanoparticles were then purified from 8% native PAGE gel.

Competition assays and radiolabel chasing

Competition experiments were carried out in the presence of urea and at different temperatures as a function of time. The Cy3 labeled 3WJ-pRNA core $[ab*c]_{3WJ}$ was constructed using three RNA oligos, a_{3wj}, Cy3-b_{3wj}, and c_{3wj} mixed at 1:1:1 molar ratio in DEPC treated water or TMS buffer.

Presence of urea—The concentration of the labeled $[ab*c]_{3WJ}$ was fixed while unlabeled b_{3WJ} was incubated with the labeled $[ab*c]_{3WJ}$ for 30-min at room temperature in presence of variable concentrations of urea (0–6M). The samples were then loaded onto 16% native gel. Two concentration ratios were evaluated: $[ab*c]_{3WJ}$: unlabeled b_{3WJ} = 1:1 and 1:5.

Different temperatures—The concentration of the labeled $[ab*c]_{3WJ}$ was fixed, while varying concentration ratios of unlabeled b_{3WJ} (1:0–1:1000) were incubated with the labeled $[ab*c]_{3WJ}$ for 30-min at 25°C, 37°C, and 55°C, respectively, before loaded onto 16% native gel.

Dilution assay to test dissociation at extremely low concentrations—The stability of the 3WJ-pRNA complex harboring three monomeric pRNA was evaluated by radiolabel assays. The purified [^{32}P]-complexes were serial diluted from 40–160 pM in TMS buffer, and then loaded onto 8% native PAGE gel.

Melting Experiments

The melting experiments were conducted by monitoring the fluorescence of the 3WJ RNAs using the LightCycler® 480 Real-Time PCR System (Roche). 1X SYBR Green I dye (Invitrogen) (emission 465–510nm), which binds double-stranded nucleic acids, but not single-stranded ones was used for all the experiments. The respective RNA oligonucleotides were mixed at room temperature in physiological TMS buffer. The 3WJ RNA samples were slowly cooled from 95°C to 20°C at the ramping rate of 0.11°C/sec. Data was analyzed by the LightCycler® 480 Software using the first derivative of the melting profile. The T_m value represents the mean and standard deviation from 3 independent experiments.

HBV ribozyme activity assay

HBV ribozyme is an RNA enzyme that cleaves the genomic RNA of the Hepatitis B Virus genome[11]. The HBV RNA substrate was radiolabeled by [α-^{32}P] UTP (PerkinElmer, Inc) and incubated with the 3WJ-pRNA or 3WJ-5S rRNA core harboring HBV ribozyme at 37°C for 60 mins in a buffer containing 20 mM $MgCl_2$, 20 mM NaCl, and 50 mM Tris-HCl, pH 7.5. The pRNA/HBV ribozyme served as a positive control[11], and 3WJ RNA harboring MD aptamer was used as a negative control (Fig. 4). The samples were then loaded on 8M urea/10% PAGE gel for autoradiograph.

Malachite green (MG) aptamer fluorescence assay

3WJ-pRNA or 3WJ-5S rRNA trivalent RNA nanoparticles harboring MG binding aptamer (100 nM)[30] was mixed with MG (2 μM) in binding buffer containing 100 mM KCl, 5 mM $MgCl_2$, and 10 mM HEPES (pH 7.4) and incubated at room temperature for 30 mins (Fig. 4f, g). The fluorescence was measured using a fluorospectrometer (Horiba Jobin Yvon), excited at 475-nm (540–800 nm scanning for emission) and 615-nm (625–800 nm scanning for emission).

Methods for the synthesis and purification of pRNA; the construction and purification of pRNA complexes; the serum stability assays; flow cytometry analysis of folate mediated cell binding; the confocal microscopy imaging; the assay for the silencing of genes in cancer cell model; the stability and systemic pharmacokinetic analysis in animals[49]; the targeting of tumor xenograft by systemic injection in animals[49]; and the AFM imaging[50] can be found in Supplementary Information Section.

Supplementary Material

Refer to Web version on PubMed Central for supplementary material.

Acknowledgments

The research was mainly supported by NIH grants EB003730, GM059944 and CA151648 to P.G., who is also a cofounder of Kylin Therapeutics, Inc. We thank Luda Shlyakhtenko and Yuri Lyubchenko for AFM images via the Nanoimaging Core Facility supported by NIH SIG program, and UNMC Program of ENRI; Nourtan Abdeltawab and Zhenqi Zhu from Malak Kotb's lab at University of Cincinnati for help with the qRT-PCR assays.

References

1. Seeman NC. Nanomaterials based on DNA. Annu Rev Biochem. 2010; 79:65–87. [PubMed: 20222824]
2. Guo P. The emerging field of RNA nanotechnology. Nat Nanotechnol. 2010; 5:833–842. [PubMed: 21102465]
3. Guo P, et al. Inter-RNA interaction of phage phi29 pRNA to form a hexameric complex for viral DNA transportation. Mol Cell. 1998; 2:149–155. [PubMed: 9702202]
4. Shukla GC, et al. A Boost for the Emerging Field of RNA Nanotechnology. ACS Nano. 2011; 5:3405–3418. [PubMed: 21604810]
5. Cruz JA, Westhof E. The Dynamic Landscapes of RNA Architecture. Cell. 2009; 136:604–609. [PubMed: 19239882]
6. Jaeger L, Verzemnieks EJ, Geary C. The UA_handle: a versatile submotif in stable RNA architectures. Nucleic Acids Res. 2009; 37:215–230. [PubMed: 19036788]
7. Fire A, et al. Potent and specific genetic interference by double-stranded RNA in Caenorhabditis elegans. Nature. 1998; 391:806–811. [PubMed: 9486653]
8. Khaled A, Guo S, Li F, Guo P. Controllable Self-Assembly of Nanoparticles for Specific Delivery of Multiple Therapeutic Molecules to Cancer Cells Using RNA Nanotechnology. Nano Letters. 2005; 5:1797–1808. [PubMed: 16159227]
9. Guo S, Tschammer N, Mohammed S, Guo P. Specific delivery of therapeutic RNAs to cancer cells via the dimerization mechanism of phi29 motor pRNA. Hum Gene Ther. 2005; 16:1097–1109. [PubMed: 16149908]
10. Guo S, Huang F, Guo P. Construction of folate-conjugated pRNA of bacteriophage phi29 DNA packaging motor for delivery of chimeric siRNA to nasopharyngeal carcinoma cells. Gene Ther. 2006; 13:814–820. [PubMed: 16482206]

11. Hoeprich S, et al. Bacterial virus phi29 pRNA as a hammerhead ribozyme escort to destroy hepatitis B virus. Gene Ther. 2003; 10:1258–1267. [PubMed: 12858191]
12. Sarver NA, et al. Ribozymes as potential anti-HIV-1 therapeutic agents. Science. 1990; 247:1222–1225. [PubMed: 2107573]
13. Liu H, et al. Phi29 pRNA Vector for Efficient Escort of Hammerhead Ribozyme Targeting Survivin in Multiple Cancer Cells. Cancer Biol Ther. 2007; 6:697–704. [PubMed: 17426446]
14. Winkler WC, et al. Control of gene expression by a natural metabolite-responsive ribozyme. Nature. 2004; 428:281–286. [PubMed: 15029187]
15. Mulhbacher J, St-Pierre P, Lafontaine DA. Therapeutic applications of ribozymes and riboswitches. Curr Opin Pharmacol. 2010; 10:551–556. [PubMed: 20685165]
16. Chen Y, et al. Nanoparticles modified with tumor-targeting scFv deliver siRNA and miRNA for cancer therapy. Mol Ther. 2010; 18:1650–1656. [PubMed: 20606648]
17. Pegtel DM, et al. Functional delivery of viral miRNAs via exosomes. Proc Natl Acad Sci U S A. 2010; 107:6328–6333. [PubMed: 20304794]
18. Ye X, Liu Z, Hemida M, Yang D. Mutation Tolerance and Targeted Delivery of Anti-Coxsackievirus Artificial MicroRNAs Using Folate Conjugated Bacteriophage Phi29 pRNA. PLoS ONE. 2011 In Press.
19. Chen C, Guo P. Magnesium-induced conformational change of packaging RNA for procapsid recognition and binding during phage phi29 DNA encapsidation. J Virol. 1997; 71:495–500. [PubMed: 8985376]
20. Chen C, Sheng S, Shao Z, Guo P. A dimer as a building block in assembling RNA: A hexamer that gears bacterial virus phi29 DNA-translocating machinery. J Biol Chem. 2000; 275(23):17510–17516. [PubMed: 10748150]
21. Guo P, Erickson S, Anderson D. A small viral RNA is required for *in vitro* packaging of bacteriophage phi29 DNA. Science. 1987; 236:690–694. [PubMed: 3107124]
22. Reid RJD, Bodley JW, Anderson D. Characterization of the prohead-pRNA interaction of bacteriophage phi29. J Biol Chem. 1994; 269:5157–5162. [PubMed: 8106496]
23. Zhang CL, Lee CS, Guo P. The proximate 5′ and 3′ ends of the 120-base viral RNA (pRNA) are crucial for the packaging of bacteriophage ϕ29 DNA. Virology. 1994; 201:77–85. [PubMed: 8178491]
24. Shu D, Zhang H, Jin J, Guo P. Counting of six pRNAs of phi29 DNA-packaging motor with customized single molecule dual-view system. EMBO J. 2007; 26:527–537. [PubMed: 17245435]
25. Xiao F, Moll D, Guo S, Guo P. Binding of pRNA to the N-terminal 14 amino acids of connector protein of bacterial phage phi29. Nucleic Acids Res. 2005; 33:2640–2649. [PubMed: 15886394]
26. Shu D, et al. Bottom-up assembly of RNA arrays and superstructures as potential parts in nanotechnology. Nano Lett. 2004; 4:1717–1723. [PubMed: 21171616]
27. Zhang CL, Trottier M, Guo PX. Circularly permuted viral pRNA active and specific in the packaging of bacteriophage Phi29 DNA. Virology. 1995; 207:442–451. [PubMed: 7533964]
28. Carlson RD, Olins AL, Olins DE. Urea denaturation of chromatin periodic structure. Biochemistry. 1975; 14:3122–3125. [PubMed: 1148192]
29. Pagratis NC. Rapid preparation of single stranded DNA from PCR products by streptavidin induced electrophoretic mobility shift. Nucleic Acids Res. 1996; 24:3645–3646. [PubMed: 8836196]
30. Baugh C, Grate D, Wilson C. 2.8 A crystal structure of the malachite green aptamer. J Mol Biol. 2000; 301:117–128. [PubMed: 10926496]
31. Lu Y, Low PS. Folate-mediated delivery of macromolecular anticancer therapeutic agents. Adv Drug Deliv Rev. 2002; 54:675–693. [PubMed: 12204598]
32. Ambrosini G, Adida C, Altieri DC. A novel anti-apoptosis gene, survivin, expressed in cancer and lymphoma. Nat Med. 1997; 3:917–921. [PubMed: 9256286]
33. Soutschek J, et al. Therapeutic silencing of an endogenous gene by systemic administration of modified siRNAs. Nature. 2004; 432:173–178. [PubMed: 15538359]
34. Behlke MA. Progress towards in vivo use of siRNAs. Mol Ther. 2006; 13:644–670. [PubMed: 16481219]

35. Chen C, Zhang C, Guo P. Sequence requirement for hand-in-hand interaction in formation of pRNA dimers and hexamers to gear phi29 DNA translocation motor. RNA. 1999; 5:805–818. [PubMed: 10376879]
36. de la PM, Dufour D, Gallego J. Three-way RNA junctions with remote tertiary contacts: a recurrent and highly versatile fold. RNA. 2009; 15:1949–1964. [PubMed: 19741022]
37. Lilley DM. Structures of helical junctions in nucleic acids. Q Rev Biophys. 2000; 33:109–159. [PubMed: 11131562]
38. Afonin KA, et al. In vitro assembly of cubic RNA-based scaffolds designed in silico. Nat Nanotechnol. 2010; 5:676–682. [PubMed: 20802494]
39. Lescoute A, Westhof E. Topology of three-way junctions in folded RNAs. RNA. 2006; 12:83–93. [PubMed: 16373494]
40. Leontis NB, Westhof E. Analysis of RNA motifs. Curr Opin Struct Biol. 2003; 13:300–308. [PubMed: 12831880]
41. Honda M, Beard MR, Ping LH, Lemon SM. A phylogenetically conserved stem-loop structure at the 5′ border of the internal ribosome entry site of hepatitis C virus is required for cap-independent viral translation. J Virol. 1999; 73:1165–1174. [PubMed: 9882318]
42. Wakeman CA, Ramesh A, Winkler WC. Multiple metal-binding cores are required for metalloregulation by M-box riboswitch RNAs. J Mol Biol. 2009; 392:723–735. [PubMed: 19619558]
43. Kulshina N, Edwards TE, Ferre-D'Amare AR. Thermodynamic analysis of ligand binding and ligand binding-induced tertiary structure formation by the thiamine pyrophosphate riboswitch. RNA. 2010; 16:186–196. [PubMed: 19948769]
44. Diamond JM, Turner DH, Mathews DH. Thermodynamics of three-way multibranch loops in RNA. Biochemistry. 2001; 40:6971–6981. [PubMed: 11389613]
45. Klostermeier D, Millar DP. Helical junctions as determinants for RNA folding: origin of tertiary structure stability of the hairpin ribozyme. Biochemistry. 2000; 39:12970–12978. [PubMed: 11041862]
46. Rettberg CC, et al. A three-way junction and constituent stem-loops as the stimulator for programmed -1 frameshifting in bacterial insertion sequence IS911. J Mol Biol. 1999; 286:1365–1378. [PubMed: 10064703]
47. Liu B, Diamond JM, Mathews DH, Turner DH. Fluorescence competition and optical melting measurements of RNA three-way multibranch loops provide a revised model for thermodynamic parameters. Biochemistry. 2011; 50:640–653. [PubMed: 21133351]
48. Mathews DH, Turner DH. Experimentally derived nearest-neighbor parameters for the stability of RNA three- and four-way multibranch loops. Biochemistry. 2002; 41:869–880. [PubMed: 11790109]
49. Abdelmawla S, et al. Pharmacological Characterization of Chemically Synthesized Monomeric pRNA Nanoparticles for Systemic Delivery. Molecular Therapy. 2011 In Press.
50. Lyubchenko YL, Shlyakhtenko LS. AFM for analysis of structure and dynamics of DNA and protein-DNA complexes. Methods. 2009; 47:206–213. [PubMed: 18835446]

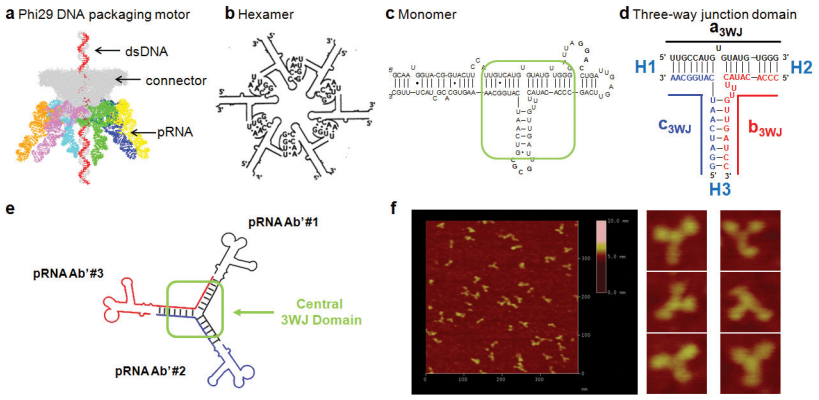

Figure 1. Sequence and secondary structure of phi29 DNA-packaging RNA (pRNA)

a, Illustration of the phi29 packaging motor geared by six pRNAs (orange, pink, light blue, green, dark blue and yellow structures). **b**, Schematic showing a pRNA hexamer assembled through hand-in-hand interactions of six pRNA monomers. **c**, Sequence of pRNA monomer Ab′. Green box: central 3WJ domain. Uppercase and lowercase letters in Ab′ represent right- and left-hand loops, respectively. **d**, The 3WJ domain composed of three RNA oligomers in black, blue and red. Helical segments are represented as H1, H2, H3. **e**, A trivalent RNA nanoparticle consisting of three pRNA molecules bound at the 3WJ-pRNA core sequence (red, black and blue) and its accompanying AFM images (**f**). Ab′ indicates non-complementary loops[35].

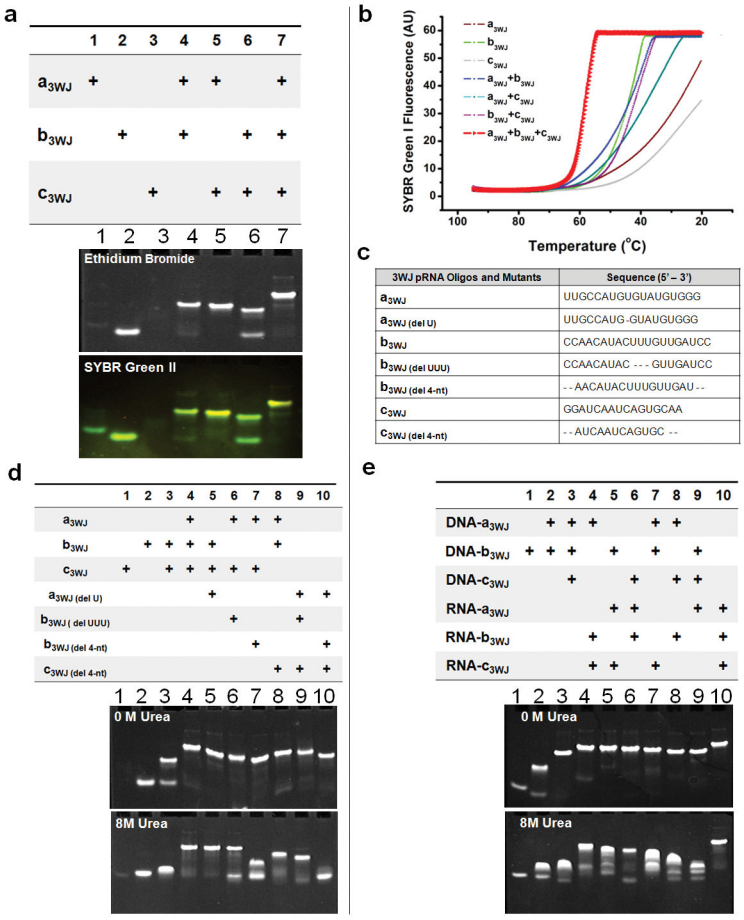

Figure 2. Assembly and stability studies of 3WJ-pRNA

In tables, '+' indicates the presence of the strand in samples of the corresponding lanes. **a**, 15% native PAGE showing the assembly of the 3WJ core, stained by EB (upper) and SYBR Green II (lower). **b**, Melting curves for the assembly of the 3WJ core. The melting curves for the individual strands (brown, green, silver), two-strand combinations (blue, cyan, pink), and three-strand combination (red) are shown. **c**, Oligo sequences of 3WJ-pRNA cores and mutants. "del U"-deletion of U bulge; "del UUU"-deletion of UUU bulge; "del 4-nt"-deletion of 2-nucleotides at 3′ and 5′ ends, respectively. **d**, Length requirements for the assembly of 3WJ cores and stability assays by urea denaturation. **e**, Comparison of DNA and RNA 3WJ-core in native and urea gel.

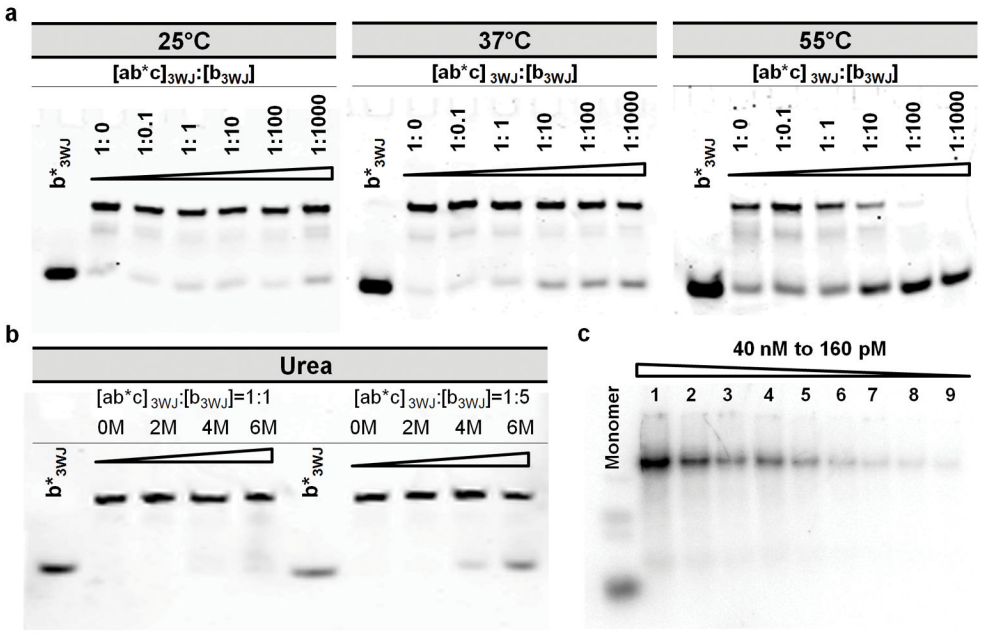

Figure 3. Competition and dissociation assays of 3WJ-pRNA

a, Temperature effects on the stability of 3WJ-pRNA core, denoted $[ab^*c]_{3WJ}$ evaluated by 16% native gel. Fixed concentration of Cy3 labeled $[ab^*c]_{3WJ}$ was incubated with varying concentration of unlabeled b_{3WJ} at 25°C, 37°C, and 55°C. **b,** Urea denaturing effects on the stability of $[ab^*c]_{3WJ}$ evaluated by 16% native gel. Fixed concentration of labeled $[ab^*c]_{3WJ}$ was incubated with unlabelled b_{3WJ} at ratios of 1:1 and 1:5 in the presence of 0–6M urea at 25°C. **c,** Dissociation assay for the [^{32}P]-3WJ-pRNA complex harboring three monomeric pRNA by 2-fold serial dilution (lanes 1–9). Monomer unit is shown on the left.

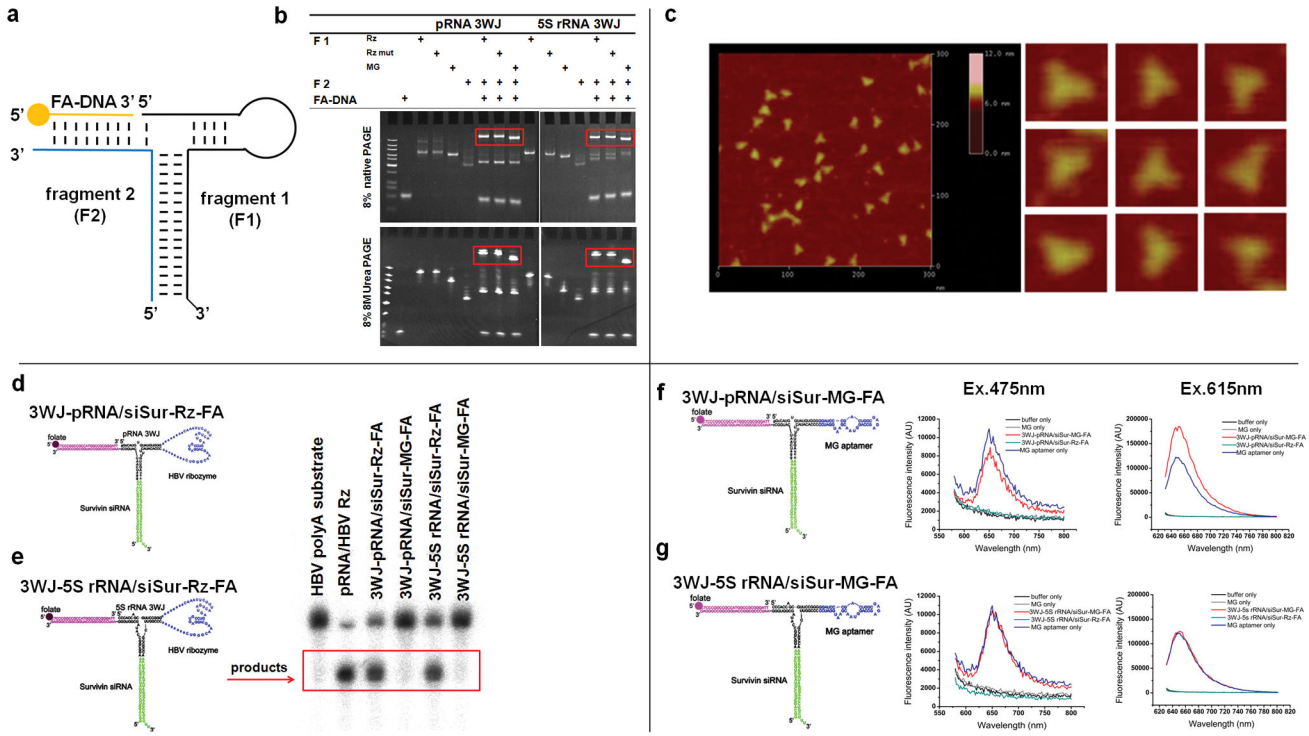

Figure 4. Construction of multi-module RNA nanoparticles harboring siRNA, ribozyme, and aptamer

a-c, Assembly of RNA nanoparticles with functionalities using the 3WJ-pRNA and 3WJ-5S rRNA as scaffolds. **a,** Illustration; **b,** 8% native (upper) and denaturing (lower) PAGE gel; **c,** AFM images of 3WJ-pRNA-siSur-rZ-FA nanoparticles. **d–e**, Assessing the catalytic activity of the Hepatitis B virus (HBV) ribozyme incorporated into the 3WJ-pRNA **(d)** and 3WJ-5S rRNA **(e)** cores, evaluated in 10% 8M Urea PAGE. The cleaved RNA product is boxed. Positive control: pRNA/HBV-Rz; Negative control: 3WJ-RNA/siSur-MG-FA. **f–g**, Functional assay of the MG (malachite green) aptamer incorporated in RNA nanoparticles using the 3WJ-pRNA **(f)** and 3WJ-5S rRNA **(g)** cores. MG fluorescence was measured using excitation wavelengths 475 and 615nm.

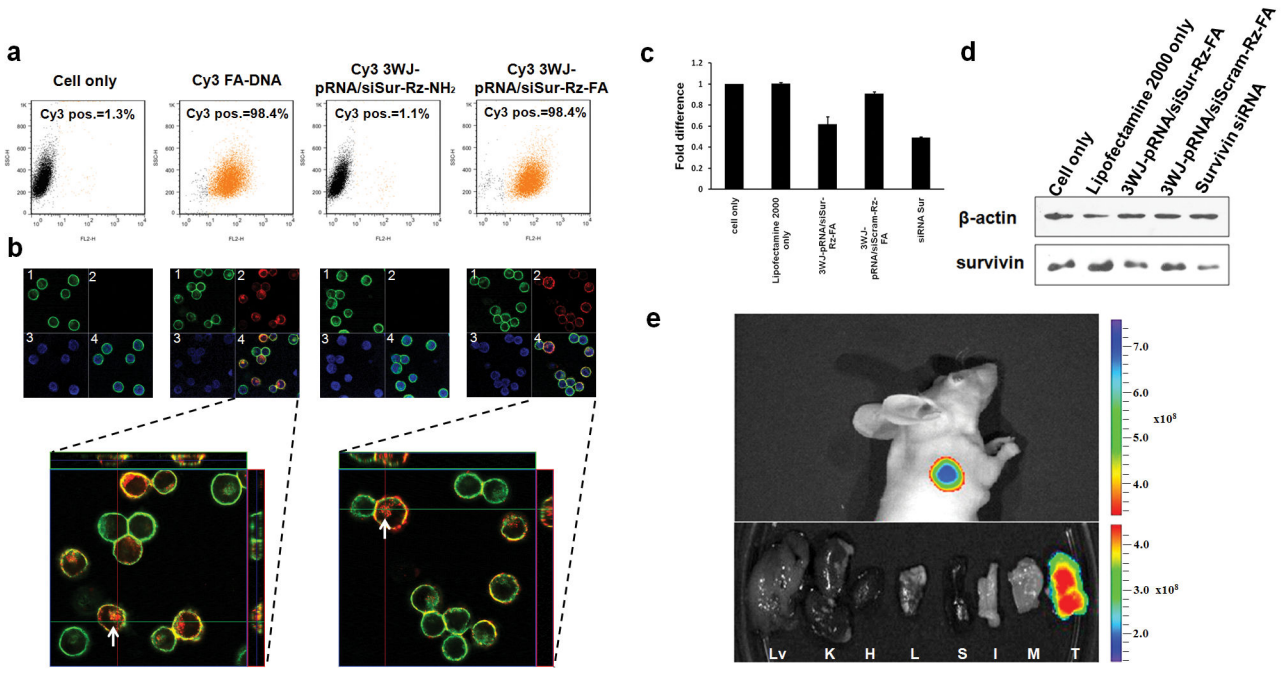

Figure 5. ***In vitro*** **and** ***in vivo*** **binding and entry of 3WJ-pRNA nanoparticles into targeted cells**

a, Flow cytometry revealed the binding and specific entry of fluorescent-[3WJ-pRNA-siSur-rZ-FA] nanoparticles into folate receptor positive (FA^+) cells. Positive and negative controls were Cy3-FA-DNA and Cy3-[3WJ-pRNA-siSur-rZ-NH_2] (without FA), respectively. **b,** Confocal images showed targeting of FA^+-KB cells by co-localization (overlap, 4) of cytoplasma (green, 1) and RNA nanoparticles (red, 2) (magnified, bottom panel). Blue–nuclei, 3. **c–d**, Target gene knock-down effects showed by **(c)** qRT-PCR with GADPH as endogenous control and by **(d)** Western blot assay with β–actin as endogenous control. **e,** 3WJ-pRNA nanoparticles target FA^+ tumor xenografts upon systemic administration in nude mice. Upper panel: whole body; Lower panel: organ imaging; Lv=liver; K=kidney; H=heart; L=lung; S=spleen; I=intestine; M=muscle; T=tumor). Scale: Fluorescent Intensity.

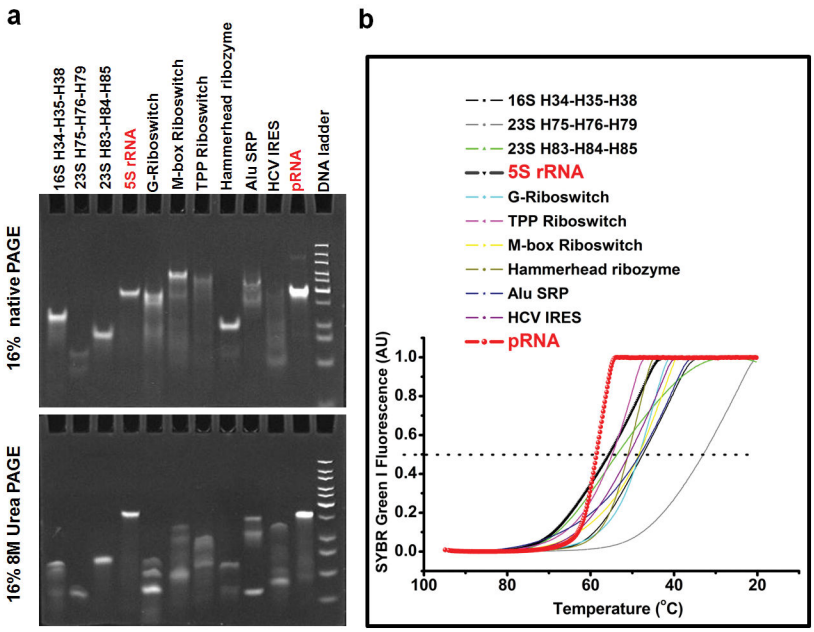

Figure 6. Comparison of different 3WJ-RNA core

a, Assembly and stability of 11 3WJ-RNA core motifs assayed in 16% native (upper) and 16% 8M Urea (lower) PAGE gel. **b,** Melting curves for each of the 11 RNA 3WJ core motifs assembled from three oligos for each 3WJ motif under the physiological buffer TMS. Please refer to the Table 1 for the respective T_m values.

Nat Nanotechnol. Author manuscript; available in PMC 2012 April 01.

Table 1

Comparison of biophysical properties of various 3WJ cores

Family	Name	Sequence 5′-3′	Assembly of 3WJ-RNA Core		Assembly of 3WJ- pRNA with three pRNA monomers		T_m(°C)
			Native Gel	8M Urea Denaturing Gel	Native Gel	8M Urea Denaturing Gel	TMS Buffer
A 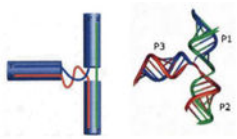	16s H34-H35-H38	a) GGG GAC GAC GUC b) CGA GCG CAA CCC CC c) GUC GUC AGC UCG	Weak	No	Yes	No	45.3 ± 6.7
	23s H75-H76- H79	a) GAG GAC ACC GA b) GGC UCU CAC UC c) UCG CUG AGC C	No	No	No	No	33.3 ± 0.6
B 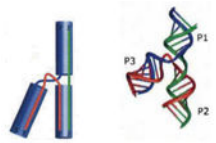	23s H83-H84- H85	a) AGC AAA AGA U b) CCC GGC GAA GAG UG c) AUC UCA GCC GGG	No	No	No	No	53.7 ± 0.6
C 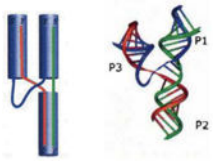	5S rRNA	a) CCC GGU UCG CCG CCA b) CCC ACC AGC GUU CCG GG c) AGG CGG CCA UAG CGG UGG G	Very Strong	Very Strong	Yes	Yes	54.3 ± 3.1
	G- Riboswitch (Type I)	a) GGA CAU AUA AUC GCG UG b) AUG UCC GAC UAU GUC C c) CAC GCA AGU UUC UAC CGG GCA	Medium	No	Yes	No	46.0 ± 3.5
	TPP Riboswitch (Type II)	a) GCG ACU CGG GGU GCC CUU C b) GAA GGC UGA GAA AUA CCC GUA UCA CCU GAU CUG G c) CCA GCG UAG GGA AGU CGC	Strong	No	Yes	No	52.0 ± 4.4
	M-box Riboswitch (Type II)	a) GAC GCC AAU GGG UCA ACA GAA AUC AUC G b) AGG UGA UUU UUA AUG CAG CU c) ACG CUG CUG CCC AAA AAU GUC	Strong	No	Yes	No	45.3 ± 5.5
	Hammerhead ribozyme	a) CUG UCA CCG GAU b) GGA CGA AAC AG c) UUC CGG UCU GAU GAG UCC	No	No	No	No	49.7 ± 1.5
	Alu SRP	a) GGG CCG GGC GCG GU b) UCG GGA GGC UC c) GGC GCG CGC CUG UAG UCC CAG C	No	No	No	No	45.3 ± 4.6
Unknown	HCV	a) UCA UGG UGU UCC GGA AAG CGC	No	No	No	No	49.7 ± 1.5

Family	Name	Sequence 5′-3′	Assembly of 3WJ-RNA Core		Assembly of 3WJ- pRNA with three pRNA monomers		T_m(°C)
			Native Gel	8M Urea Denaturing Gel	Native Gel	8M Urea Denaturing Gel	TMS Buffer
		b) GUG AUG AGC CGA UCG UCA GA c) UCU GGU GAU ACC GAG A					
	pRNA	a) UUG CCA UGU GUA UGU GGG b) CCC ACA UAC UUU GUU GAU CC c) GGA UCA AUC AUG GCA A	Very Strong	Very Strong	Yes	Yes	58.0 ± 0.5

Note: The sequences of the 3WJ cores were obtained from References [35,39,41–43]. Families A, B and C are based on Lescoute and Westhof classification [39]. Other 14 3WJ cores that were not practical for thorough investigations are listed in Supplementary Table 2.